BABEȘ-BOLYAI UNIVERSITY
Faculty of Physics
Doctoral School of Physics

Ph.D. Thesis

A novel solvothermal synthesis method for reduced graphene oxide and its potential in the development of new polymer-based composites for thermal interface materials

Raluca Țărcan

Scientific Coordinator
C.S.I Dr. Habil. Ioan Botiz

Cluj-Napoca
2024

Table of Contents

Aims and Motivation

Thermal interface materials (TIMs) are effective materials placed and the interface of two components in an electronic assembly to enhance the thermal management of the system and to efficiently dissipate the excessive heat. Polymers are often used in the development of TIMs, however most of them present low thermal conductivity. Therefore, filler materials with excellent thermal properties are required in order to improve the thermal efficiency of the polymer-based composites used in such applications.

Reduced graphene oxide presents outstanding thermal properties very similar with those of pristine graphene, thus making it a great candidate to be used as a filler material in the development of new polymer-based composites for thermal interface materials.

However, while most polymers are easily dispersed and processed in solution, reduced graphene oxide comes with some challenges, as often times the agglomeration of the flakes occurs in solution due to strong Van der Waals interactions.

Therefore, the scope of this thesis was to develop new thermal interface materials based on thermoconductive polymer composites, while exploring the processability of reduced graphene oxide in water and organic solvents. We aimed to find a common solvent suitable for the processing of both polymers and RGO. In this process we strived to (1) maximize the concentration in which RGO could be obtained and stabilized in water using a microwave-assisted hydrothermal synthesis, and (2) to obtain a RGO stable dispersion in an organic solvent in high concentration for blending it with the polymeric solution. Nonetheless, the performance of the polymer/RGO composite was evaluated and demonstrated for developing new thermal interface materials.

The Structure of the Thesis

This thesis is structured in two main sections (**Part I - Literature Review** and **Part II - Original Contributions**) and it follows a clear thread from the basic unit of graphene-based materials – the carbon atom – to the complexity of their structure and properties, their synthesis methods, and their practical applicability, with a particular emphasis on reduced graphene oxide (RGO).

Chapter 1 presents a literature review that summarizes an up-to-date knowledge on graphene, GO, and RGO. This chapter focuses on the most commonly used synthesis methods, how they tailor the structure of the resulting materials, and, of course, the relationship between the structure and the unique and outstanding properties that they possess.

Chapter 2 presents a state-of-the art on the vast applicability of RGO in all aspects of life. Starting from energy-storage applications and optoelectronics, to bioapplications and nanomedicine, reduced graphene oxide has proved itself as an excellent alternative due to its outstanding properties similar to those of pristine graphene.

Chapter 3 is the first chapter to discuss the research results related to this thesis. Here we explore the processability of RGO in water and we optimize the microwave-assisted hydrothermal synthesis method of RGO with the aid of hydrazine hydrate and ammonia. We strive to maximize the concentration in which RGO can be synthesized using this method, and we investigate the behavior of RGO dispersion in water when employed for the thin film deposition by spin-casting and drop-casting.

In **Chapter 4** we present a new synthesis method for RGO in *N,N*-dimethilformamide (DMF). Our proposed method is time-efficient and facile, and involves the microwave-assisted reduction of a GO dispersion in DMF at 120 °C, in only 30 minutes, without using any additional reducing or stabilizing agents. This successfully led to homogenous and stable dispersions of RGO in DMF. The success of this synthesis method was confirmed by an in-depth analysis of the as-obtained material using spectroscopic and microscopic analysis methods.

In **Chapter 5** we demonstrate further the applicability of the synthesis method deployed in Chapter 4. Here, we blend the RGO dispersion in DMF with poly(methyl methacrylate) (PMMA) in order to obtain PMMA/RGO composite thin films with improved thermal properties. While investigating the thermal properties of the produced composite, we have noticed an outstanding increase in thermal conductivity up to 210% for PMMA/RGO composite with a concentration of 0.5 wt% RGO. This result opens new opportunities to use this type of composites as thermal interface materials for automotive industries.

In **Appendices** we have included some supplementary information related to the development of the synthesis method for RGO in DMF (Appendix A), and the simulation results obtained for the PMMA/RGO composite demonstrating its potential performance as a thermal interface material (Appendix B).

PART I

LITERATURE REVIEW

Chapter 1. Overview of Graphene, Graphene Oxide, and Reduced Graphene Oxide

1.1. History and Definitions

For a very long time it was believed that the two-dimensional allotrope of carbon (Figure 1.1.1.), can exist only theoretically, being thermodynamically instable. However, in 2004 Professors Andre Geim and Konstantin Novoselov performed the mechanical exfoliation of graphite using a simple scotch tape method and have successfully isolated for the first time an individual sheet of graphene [1]. Nonetheless, in 2010 they have been awarded the Nobel Prize for this outstanding discovery and it represented the start of a new era: “The Graphene Era”.

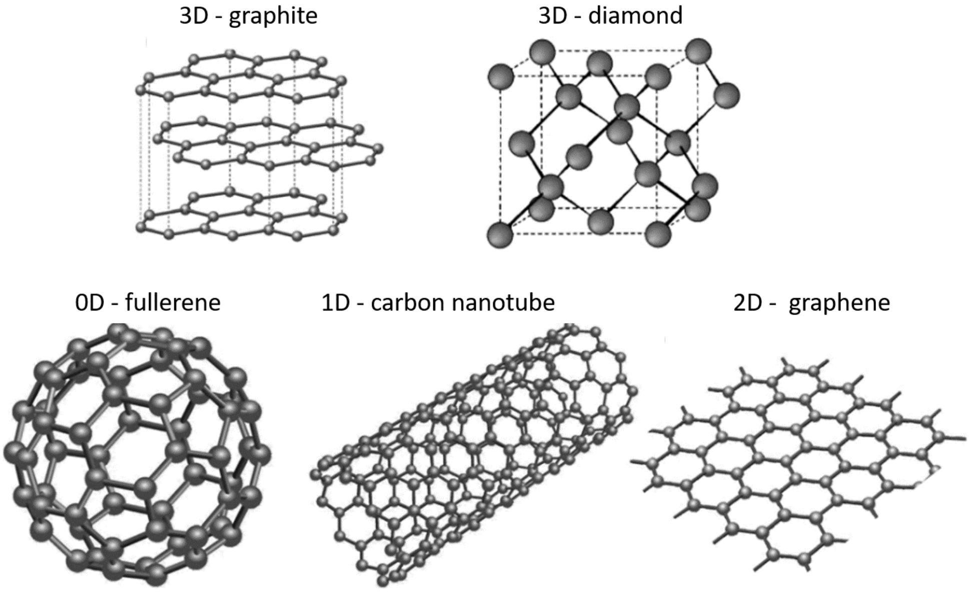

Figure 1.1.1. Different allotropes of carbon. Reproduced with permission from [2]

Graphene can be defined as a two-dimensional crystal having sp^2-hybridized carbon atoms disposed in a hexagonal, honeycomb-like lattice. It displays excellent optical, electronical, and mechanical properties, which made it gain the name of “wonder material”. Nonetheless, graphene can be considered the foundational unit of the other carbon allotropes, such as fullerenes, carbon nanotubes, and graphite, but also for its derivatives: graphene oxide (GO) and reduced graphene oxide (RGO).

1.2. Synthesis Methods

The synthesis method used to produce graphene must be rigorously controlled in order to obtain a graphene with ideal structure and, in consequence, with ideal properties. In general, the synthesis methods for graphene are divided in two important categories: ***bottom-up*** and ***top-down*** (Figure 1.2.1).

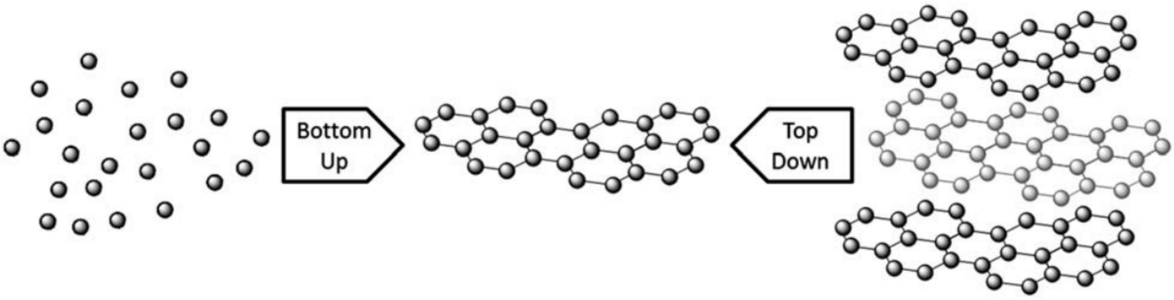

Figure 1.2.1. Simple scheme of bottom-up and top-down approaches in graphene synthesis. Reproduced with permission from [3].

The ***bottom-up*** approach includes methods such as chemical vapor deposition (CVD) or epitaxial growth, and it employs the utilization of different carbon-based precursors, such as hydrocarbons [4-8] or carbon bearing-gases [4, 9, 10]. Using complex equipment and extreme conditions, such as high temperatures or pressure, the carbon atoms will nucleate on a substrate and will form the hexagonal sp^2 carbon network of graphene. These methods will lead to the formation of a large size graphene with very few defects and excellent properties [11], but in rather small quantities. The procedures and the equipment are complex and expensive, and thus many scientists prefer using other approaches.

Top-down methods refer to the exfoliation of graphite using mechanical, electrochemical, or chemical approaches [12, 13]. These methods lead, in general, to graphene derivatives, such as graphene oxide (GO) and reduced graphene oxide (RGO), which present few more structural defects and impurities, leading to altered properties but very similar with those of pristine graphene. However, the methods are easier and cheaper, and they can be used to obtain graphene in higher quantities.

One of the most used synthesis methods for obtaining graphene and graphene derivatives is represented by the chemical oxidation-reduction approach illustrated in Figure 1.2.2.

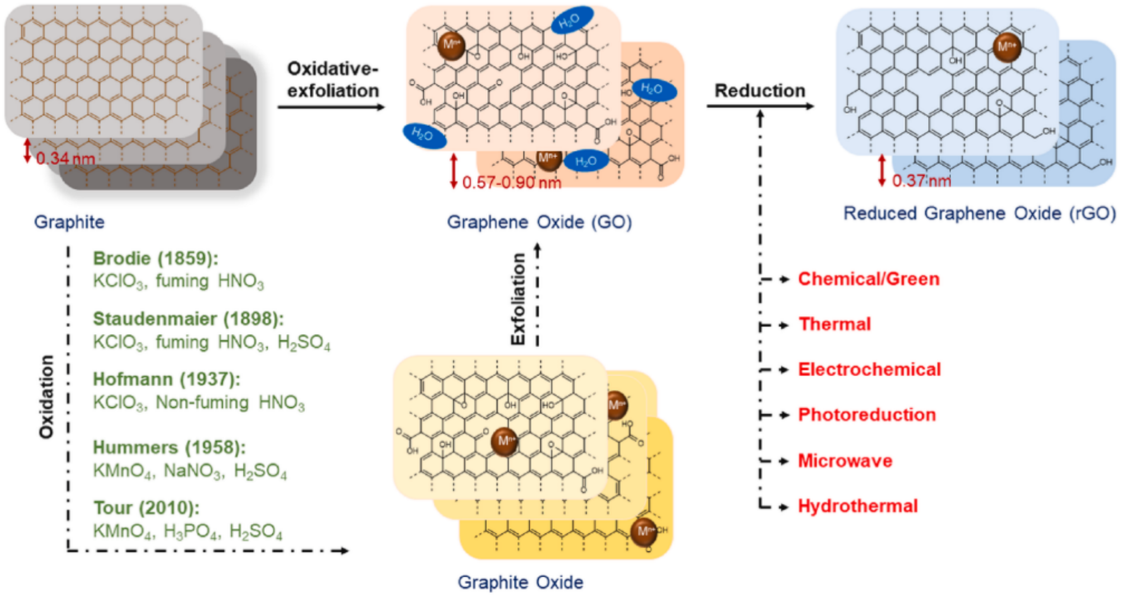

Figure 1.2.2. Schematic synthesis route of RGO through the chemical oxidation-reduction process of graphite. Reproduced with permission from [12].

The first step in this process is represented by the chemical oxidation of graphite using protocols well-known in the literature [14-21], leading to the formation of graphite oxide (GO). Further exfoliation leads to the formation of graphene oxide, which represents individual sheets of graphene with structural defects caused by the attachment of oxygen-functional groups on its surface during the oxidation process. Following a reduction process, the oxygen-containing groups are partially removed and a partial restoration of the sp^2 network occurs, leading to the formation of reduced graphene oxide (RGO), a material with excellent properties very similar with those of pristine graphene.

Controlling the parameters during the synthesis method, one can alter not only graphene's structure, but also its properties required for the desired application, making it fundamental to understand how the material properties are influenced by its structure.

1.3. Structure-Property Relationship in Graphene Derivatives

A single graphene sheet has a thickness of 0.35 nm, while the bond between two carbon atoms is ~0.142 nm. Each carbon atom presents four valence electrons. Three of them, from the orbitals 2s, $2p_x$ and $2p_y$, are involved in the in-plane σ bonds, which are forming the strong and stiff hexagonal lattice structure and are responsible for the amazing thermal and mechanical properties [22-24]. The fourth valence electrons of the carbon atoms are situated in the $2p_z$ orbitals, oriented perpendicular on the basal plane. All these electrons are delocalized, forming the π bonds, and are mainly responsible for the outstanding optical and electrical properties [25]. Additionally, the two-dimensional crystalline structure of graphene leads to a large specific surface area of ~2630 m^2 g^{-1} [26]. Despite of being one-atom thick, graphene is one hundred times stiffer than steel, having a Young's modulus of 1 TPa and a tensile strength of 130 GPa [26, 27]. The thermal conductivity of single-layer graphene can be as high as 5300 W m^{-1} K^{-1} [28], making it a great candidate for manufacturing devices that require efficient heat dissipation. The charge carriers' mobility (electrons and holes) in graphene is ~200,000 cm^2 v^{-1} s^{-1} [29, 30], thus defining its high electronic quality. Graphene is highly transparent, having an optical transmittance of 97.7%, and still absorbing 2.3% of incident light [31].

All these outstanding properties are making graphene a great candidate for a plethora of applications, especially for various electronic and optoelectronic devices.

Chapter 2. Reduced Graphene Oxide Today[1]

Reduced graphene oxide (RGO) can be defined as a graphene derivative having a heterogeneous structure presenting a basal plane made of carbon atoms disposed in a honeycomb lattice, very similar with pristine graphene. Additionally, RGO presents structural defects caused by the oxygen functional groups attached to its basal plane. Due to its structure, it possesses very similar optoelectronic, conductive, and mechanical properties as pristine graphene, making RGO an advantageous material to be used in various biological, environmental, catalytic, or sensing applications, but also for optoelectronic and storage devices. Moreover, the oxygen-containing groups attached to its surface offer RGO properties that are not characteristing to graphene, such as colloidal stability, dispersibility, and processability in aqueous solution.

This chapter includes a diversified review of RGO's applications (Figure 2.1.), with an emphasis on the relationship between the RGO synthesis, functionalization, or processing methods, enhanced composite or device functionality, and RGO's structure. The chapter is entirely adapted from our previously published work [32].

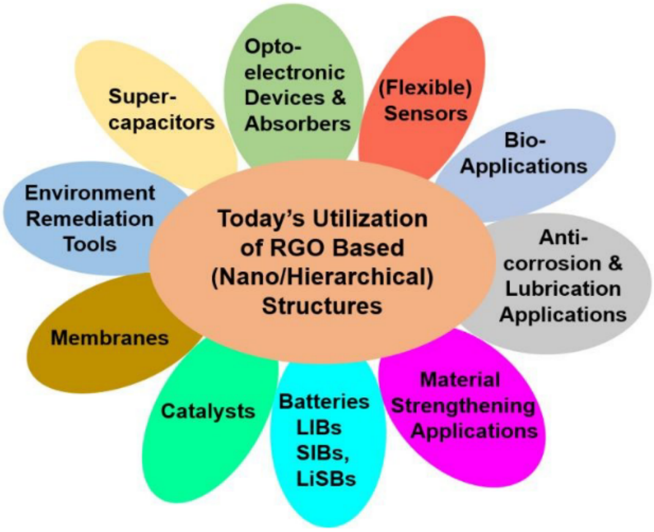

Figure 2.1. The variety of applications of RGO. Reproduced with permission from [32].

Undoubtedly, RGO demonstrates great versatility across various technological fields, finding applications in an increasing number of devices. This chapter concludes that RGO is most advantageous when incorporated in binary, ternary, or quaternary blends. RGO-based composites

---

[1] This chapter is entirely adapted from our previous publication [32] R. Tarcan, O. Todor-Boer, I. Petrovai, C. Leordean, S. Astilean, and I. Botiz, "Reduced graphene oxide today," *Journal of Materials Chemistry C,* vol. 8, pp. 1198-1224, 2020, doi: 10.1039/c9tc04916a

with complex architectures display innovative and improved structure-related properties, while they can be easily synthesized through diverse precursor structures (sheets, rods, ribbons, wires, particles, spheres, etc.) and different physical or synthetic processes (chemical reactions, thermal processes, functionalization, polymerization, etc.). The coupling of different composite components results in diverse and highly beneficial synergistic effects. Multi-component composites, particularly in sensors, mechanical, rheological, and anticorrosion applications, show an increased number of positive synergistic effects.

Furthermore, it has been shown that for efficient battery fabrication, RGO-based composites need to possess a 3D structure and porosity, facilitating charge transfers and ion diffusion processes.

To fully unleash the potential of RGO, novel synthesis and processing methods need to be developed to expand and enhance its range of properties. For example, envisioning and implementing an innovative synthetic method leading to RGO suspensions in organic solvents in high concentration could position RGO as a crucial material component in organic flexible optoelectronic devices and polymer-based composites in the future.

References:

[1] K. S. Novoselov, A. K. Geim, S. V. Morozov, D. Jiang, Y. Zhang, S. V. Dubonos, I. V. Grigorieva, and A. A. Firsov, "Electric Field Effect in Atomically Thin Carbon Films," *Science,* vol. 306, pp. 666-669, 2004, doi: doi:10.1126/science.1102896

[2] M. Scarselli, P. Castrucci, and M. De Crescenzi, "Electronic and optoelectronic nano-devices based on carbon nanotubes," *Journal of Physics: Condensed Matter,* vol. 24, p. 313202, 2012, doi: 10.1088/0953-8984/24/31/313202

[3] R. S. Edwards and K. S. Coleman, "Graphene synthesis: relationship to applications," *Nanoscale,* vol. 5, pp. 38-51, 2013, doi: 10.1039/c2nr32629a

[4] Y. Yan, F. Z. Nashath, S. Chen, S. Manickam, S. S. Lim, H. Zhao, E. Lester, T. Wu, and C. H. Pang, "Synthesis of graphene: Potential carbon precursors and approaches," *Nanotechnology Reviews,* vol. 9, pp. 1284-1314, 2020, doi: doi:10.1515/ntrev-2020-0100

[5] R. Kumar, R. K. Singh, and D. P. Singh, "Natural and waste hydrocarbon precursors for the synthesis of carbon based nanomaterials: Graphene and CNTs," *Renewable and Sustainable Energy Reviews,* vol. 58, pp. 976-1006, 2016, doi: https://doi.org/10.1016/j.rser.2015.12.120

[6] Y. Lu and X. Yang, "Molecular simulation of graphene growth by chemical deposition on nickel using polycyclic aromatic hydrocarbons," *Carbon,* vol. 81, pp. 564-573, 2015, doi: https://doi.org/10.1016/j.carbon.2014.09.091

[7] T. Liang, Y. Kong, H. Chen, and M. Xu, "From Solid Carbon Sources to Graphene," *Chinese Journal of Chemistry,* vol. 34, pp. 32-40, 2016, doi: https://doi.org/10.1002/cjoc.201500429

[8] M. I. Kairi, M. Khavarian, S. A. Bakar, B. Vigolo, and A. R. Mohamed, "Recent trends in graphene materials synthesized by CVD with various carbon precursors," *Journal of Materials Science,* vol. 53, pp. 851-879, 2018, doi: 10.1007/s10853-017-1694-1

[9] Y. M. Manawi, Ihsanullah, A. Samara, T. Al-Ansari, and M. A. Atieh, "A Review of Carbon Nanomaterials' Synthesis via the Chemical Vapor Deposition (CVD) Method," *Materials,* vol. 11, p. 822, 2018, doi:

[10] D. G. Papageorgiou, I. A. Kinloch, and R. J. Young, "Mechanical properties of graphene and graphene-based nanocomposites," *Progress in Materials Science,* vol. 90, pp. 75-127, 2017, doi: https://doi.org/10.1016/j.pmatsci.2017.07.004

[11] K. A. Madurani, S. Suprapto, N. I. Machrita, S. L. Bahar, W. Illiya, and F. Kurniawan, "Progress in Graphene Synthesis and its Application: History, Challenge and the Future Outlook for Research and Industry," *ECS Journal of Solid State Science and Technology,* vol. 9, p. 093013, 2020, doi: 10.1149/2162-8777/abbb6f

[12] N. Kumar, R. Salehiyan, V. Chauke, O. Joseph Botlhoko, K. Setshedi, M. Scriba, M. Masukume, and S. Sinha Ray, "Top-down synthesis of graphene: A comprehensive review," *FlatChem,* vol. 27, p. 100224, 2021, doi: https://doi.org/10.1016/j.flatc.2021.100224

[13] J. Y. Lim, N. M. Mubarak, E. C. Abdullah, S. Nizamuddin, M. Khalid, and Inamuddin, "Recent trends in the synthesis of graphene and graphene oxide based nanomaterials for removal of heavy metals — A review," *Journal of Industrial and Engineering Chemistry,* vol. 66, pp. 29-44, 2018, doi: https://doi.org/10.1016/j.jiec.2018.05.028

[14] B. C. Brodie, "XIII. On the atomic weight of graphite," *Philosophical Transactions of the Royal Society of London,* vol. 149, pp. 249-259, 1859, doi: doi:10.1098/rstl.1859.0013

[15] L. Staudenmaier, "Verfahren zur Darstellung der Graphitsäure," *Berichte der deutschen chemischen Gesellschaft,* vol. 31, pp. 1481-1487, 1898, doi: https://doi.org/10.1002/cber.18980310237

[16] U. Hofmann and E. König, "Untersuchungen über Graphitoxyd," *Zeitschrift für anorganische und allgemeine Chemie,* vol. 234, pp. 311-336, 1937, doi: https://doi.org/10.1002/zaac.19372340405

[17] U. Hofmann and R. Holst, "Über die Säurenatur und die Methylierung von Graphitoxyd," *Berichte der deutschen chemischen Gesellschaft (A and B Series),* vol. 72, pp. 754-771, 1939, doi: https://doi.org/10.1002/cber.19390720417

[18] W. S. Hummers, Jr. and R. E. Offeman, "Preparation of Graphitic Oxide," *Journal of the American Chemical Society,* vol. 80, pp. 1339-1339, 1958, doi: 10.1021/ja01539a017

[19] H. L. Poh, F. Šaněk, A. Ambrosi, G. Zhao, Z. Sofer, and M. Pumera, "Graphenes prepared by Staudenmaier, Hofmann and Hummers methods with consequent thermal exfoliation exhibit very different electrochemical properties," *Nanoscale,* vol. 4, pp. 3515-3522, 2012, doi: 10.1039/c2nr30490b

[20] D. C. Marcano, D. V. Kosynkin, J. M. Berlin, A. Sinitskii, Z. Sun, A. Slesarev, L. B. Alemany, W. Lu, and J. M. Tour, "Improved Synthesis of Graphene Oxide," *ACS Nano,* vol. 4, pp. 4806-4814, 2010, doi: 10.1021/nn1006368

[21] D. C. Marcano, D. V. Kosynkin, J. M. Berlin, A. Sinitskii, Z. Sun, A. S. Slesarev, L. B. Alemany, W. Lu, and J. M. Tour, "Correction to Improved Synthesis of Graphene Oxide," *ACS Nano,* vol. 12, pp. 2078-2078, 2018, doi: 10.1021/acsnano.8b00128

[22] Z. Zhen and H. Zhu, "1 - Structure and Properties of Graphene," in *Graphene*, H. Zhu, Z. Xu, D. Xie, and Y. Fang, Eds.: Academic Press, 2018, pp. 1-12.

[23] A. Bandyopadhyay, P. Dasgupta, and S. Basak, "Anisotropic Nanofillers in TPE," in *Engineering of Thermoplastic Elastomer with Graphene and Other Anisotropic Nanofillers*,

A. Bandyopadhyay, P. Dasgupta, and S. Basak, Eds., Singapore: Springer Singapore, 2020, pp. 17-99.

[24] W. Yu, L. Sisi, Y. Haiyan, and L. Jie, "Progress in the functional modification of graphene/graphene oxide: a review," *RSC Advances,* vol. 10, pp. 15328-15345, 2020, doi: 10.1039/d0ra01068e

[25] D. R. Cooper, B. D'Anjou, N. Ghattamaneni, B. Harack, M. Hilke, A. Horth, N. Majlis, M. Massicotte, L. Vandsburger, and E. Whiteway, "Experimental review of graphene," *arXiv preprint arXiv:1110.6557,* 2011, doi:

[26] Y. Zhu, S. Murali, W. Cai, X. Li, J. W. Suk, J. R. Potts, and R. S. Ruoff, "Graphene and Graphene Oxide: Synthesis, Properties, and Applications," *Advanced Materials,* vol. 22, pp. 3906-3924, 2010, doi: https://doi.org/10.1002/adma.201001068

[27] C. Lee, X. Wei, J. W. Kysar, and J. Hone, "Measurement of the Elastic Properties and Intrinsic Strength of Monolayer Graphene," *Science,* vol. 321, pp. 385-388, 2008, doi: 10.1126/science.1157996

[28] A. A. Balandin, S. Ghosh, W. Bao, I. Calizo, D. Teweldebrhan, F. Miao, and C. N. Lau, "Superior Thermal Conductivity of Single-Layer Graphene," *Nano Letters,* vol. 8, pp. 902-907, 2008, doi: 10.1021/nl0731872

[29] S. V. Morozov, K. S. Novoselov, M. I. Katsnelson, F. Schedin, D. C. Elias, J. A. Jaszczak, and A. K. Geim, "Giant Intrinsic Carrier Mobilities in Graphene and Its Bilayer," *Physical Review Letters,* vol. 100, p. 016602, 2008, doi: 10.1103/PhysRevLett.100.016602

[30] K. I. Bolotin, K. J. Sikes, Z. Jiang, M. Klima, G. Fudenberg, J. Hone, P. Kim, and H. L. Stormer, "Ultrahigh electron mobility in suspended graphene," *Solid State Communications,* vol. 146, pp. 351-355, 2008, doi: https://doi.org/10.1016/j.ssc.2008.02.024

[31] R. R. Nair, P. Blake, A. N. Grigorenko, K. S. Novoselov, T. J. Booth, T. Stauber, N. M. R. Peres, and A. K. Geim, "Fine Structure Constant Defines Visual Transparency of Graphene," *Science,* vol. 320, pp. 1308-1308, 2008, doi: 10.1126/science.1156965

[32] R. Tarcan, O. Todor-Boer, I. Petrovai, C. Leordean, S. Astilean, and I. Botiz, "Reduced graphene oxide today," *Journal of Materials Chemistry C,* vol. 8, pp. 1198-1224, 2020, doi: 10.1039/c9tc04916a

PART II

ORIGINAL CONTRIBUTIONS

Chapter 3. Reduced Graphene Oxide in Aqueous Solution

3.1. Background and Motivation

Reduced graphene oxide (RGO) presents a unique surface chemistry, with sp^2 carbon domains, responsible for the hydrophobicity of the graphitic sheets, and oxygen-functional groups attached to its surface and responsible for the hydrophilic behavior of this material. However, due to the strong Van der Waals interactions, the agglomeration of the graphitic sheets occurs, leading to a low stability in solution.

In their study, Dan Li et al. [1] have shown that while dispersed in water, GO sheets are negatively charged, as a result of ionization of the carboxylic and hydroxylic groups [2, 3]. Hence, the formation of stable GO colloids in water is dependent on hydrophilicity and electrostatic repulsion. Given that the carboxylic groups remain attached to the basal plane after the reduction process [4], they should still be charged in aqueous solution. Therefore, they have suggested that RGO dispersions could be stabilized without the aid of any stabilizing agents of functionalization, through a rigorous control of pH and electrostatic repulsion. They proposed a method for successfully obtaining stable dispersions of RGO in water in concentration of 0.05 wt.% by reducing a GO dispersion in water with hydrazine hydrate in the presence of ammonia solution, and the optimal ration of hydrazine to GO was 7:10.

Later on, the method proposed by Li et al. was streamlined by Iliut et al. [5], in a protocol where they replaced the traditional heating with the use of a microwave heating reactor. In their approach, GO was successfully reduced to RGO in 20 minutes heating at 100 °C. However, the method also led to a low concentration of RGO of only ~0.05 mg/mL.

In this chapter we aim to maximize the concentration in which RGO can be obtained in water using the microwave-assisted hydrothermal method, following the approaches discussed above.

3.2. Materials and Methods

Reducing Graphene Oxide in Water

For the reduction reaction the microwave-assisted hydrothermal method was employed. A mixture of GO dispersion in water, hydrazine hydrate and ammonia were placed in a quartz tube and introduced in an Anton Paar Monowave 300 microwave reactor, where it was heated at 100 °C for 20 minutes, with the aim to obtain RGO dispersions of 0.5, 1, 2, and 3 mg/mL. The quantities of each reactant are presented below in Table 3.2.1.

Table 3.2.1. Reactants quantities used for the reduction of GO to RGO in water, in concentrations of 0.5, 1, 2, and 3 mg/mL.

Desired concentration of RGO dispersion in water (mg/mL)	**GO 1 mg/mL (µL)**	**GO 5 mg/mL (µL)**	**Water (µL)**	**Hydrazine Hydrate 25% (µL)**	**Ammonia 28% (µL)**	**pH**
0.5	500	n/a	500	22	8	10..7
1	1000	n/a	n/a	44	16	10.9
2	n/a	400	600	88	32	11.1
3	n/a	600	400	132	48	11.2

3.3. Results and Discussion

3.3.1. Reduced Graphene Oxide Dispersions in Water

The first results we represented by the preliminary observations, showing that following the reduction process the color of the solutions changed from light brown, characteristic for GO, to black, characteristic for RGO, suggesting that the reduction process occurred. Digital images of GO solution in water and its resulting RGO dispersions of 0.5, 1, 2, and 3 mg/mL are illustrated in Figure 3.3.1.1., along with an RGO dispersion in a concentration of 0.05 mg/mL, synthesized using the method previously used in our lab [5].

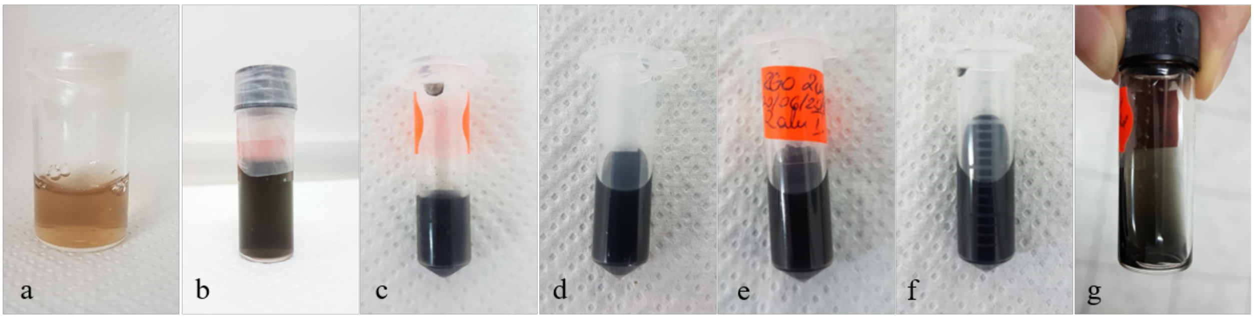

Figure 3.3.1.1. Digital photos of (**a**) GO dispersion in water and RGO dispersions in water: (**b**) 0.05 mg/mL, (**c**) 0.5 mg/mL, (**d**) 1 mg/mL, (**e**) 2 mg/mL, (**f**,**g**) 3 mg/mL.

We observed that the RGO dispersion of 0.5 mg/ml was stable and did not present any agglomeration right after the reduction, but the RGO solutions of 1, 2 and 3 mg/mL presented few flakes that could be successfully removed after centrifugation. However, the samples with RGO in higher concentration presented limited stability (<24) before the agglomeration of the flakes occurred.

However, for future characterizations, RGO dispersion 2 mg/ml was selected, as this method presented the highest reproducibility for the RGO dispersion in the highest concentration.

To confirm the success of the reduction process, we performed the UV-vis and Raman investigation for both GO and RGO (Figure 3.3.1.2.).

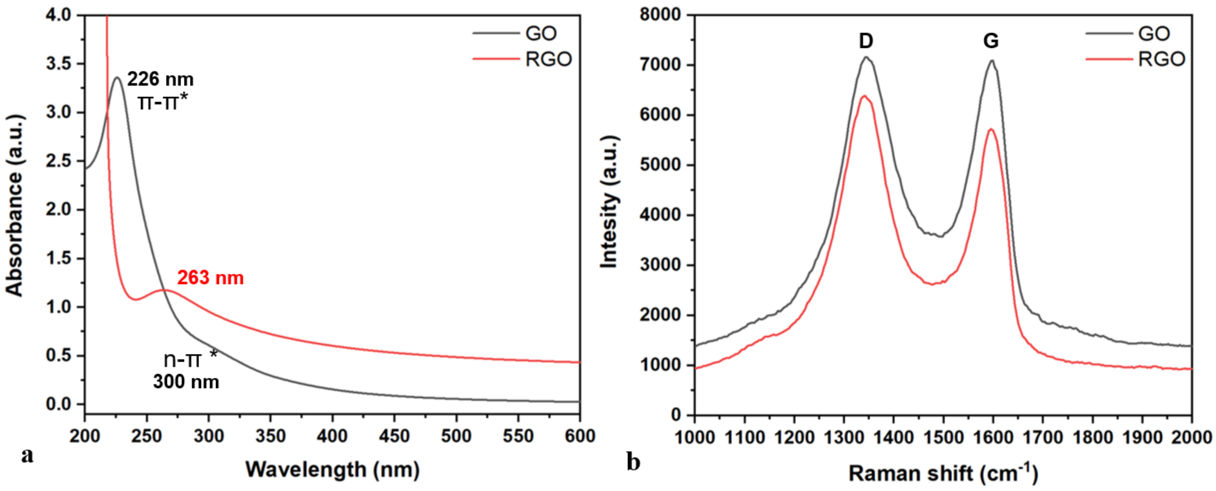

Figure 3.3.1.2. (**a**) UV-vis spectra and (**b**) Raman spectra of GO and RGO solutions in water.

The UV-vis spectra for both GO and RGO exhibit characteristic peaks corresponding to their structural particularities. For GO, the peak maximum at ~226 nm is characteristic to π-π* transitions from C=C bonds present in the aromatic structure of the graphitic basal plane, while the shoulder visible at ~300 nm is a result of the n-π* transitions characteristic to C=O bonds from oxygen functional groups present on the structure of GO [6]. After the reduction reaction not only that the color of the solution changes from brown to black, but the UV-vis spectrum is also different. The maximum absorption peak characteristic for C=C bonds appears redshifted to ~263 nm, the shoulder characteristic for C=O bonds completely disappears, and the absorption is increased throughout the entire visible and NIR range. These changes suggest that the oxygen-containing groups have been partially removed, leading to a restoration of the of the sp^2 network in the graphitic basal plane, confirming the success of the reduction process.

Raman spectra show the two bands characteristic for carbon-based structures, the D and G bands. The D band offers information regarding the defects present in sp^2 network, while the G band arises from the in-plane stretching vibrations of the C=C bonds. Following the reduction of GO, the band width is narrower, and the I_D/I_G ratio increases from 1.01 in GO to 1.12 in RGO, indicating the success of the reduction process as well, with a partial restoration of the sp^2 conjugated network.

3.3.2. Reduced Graphene Oxide Thin Films from Water Dispersions

Further investigations involved a simple study on thin films deposition from RGO water dispersions using two well-known techniques, spin-casting and drop-casting, the the film morphology was observed and characterized using optical microscopy (Figures 3.3.2.1. and 3.3.2.2.).

When using the spin-coating method (Figure 3.3.2.1.), it was observed that high rotational speeds lead to instantaneous removal of the solution droplet from the substrate, resulting in extremely thin films with small flakes randomly distributed on the substrate. On the contrary, small rotational speeds lead to the agglomeration of the RGO flakes. A better method was to start from small rotational speeds such as 200 rpm and gradually increasing to 1300 rpm until complete water evaporation occurs, while maintain each spinning step for 60 s. This led to thicker, more uniform films, however, the methods led to random distribution of RGO flakes and random film morphology.

Drop-casting of RGO at various temperatures (Figure 3.3.2.2.) gives new insights on how the processing temperature influences the film morphology. The most uniform films have been obtained at room temperature and at 50 °C, while at temperatures as high as 80–100 °C multiple defects start to appear as a result of higher water evaporation rate. For the films deposited at more than 100 °C when water evaporation occurs instantaneously, the films presented even more defects, making them unsuitable for future applications.

Analyzing the RGO thin films deposited by drop-casting at room temperature using the Atomic Force Microscopy (AFM) technique confirmed their uniform morphology with some structural features randomly distributed, together with elongated, closely packed structures formed by the agglomeration of RGO flakes (Figure 3.3.2.3.). Additionally, the thickness of the film has been approximated to several tens of nanometers.

Analyzing the RGO thin films deposited by drop-casting at room temperature using the Atomic Force Microscopy (AFM) technique confirmed their uniform morphology with some structural features randomly distributed, together with elongated, closely packed structures formed by the agglomeration of RGO flakes (Figure 3.3.2.3.). Additionally, the thickness of the film has been approximated to several tens of nanometers.

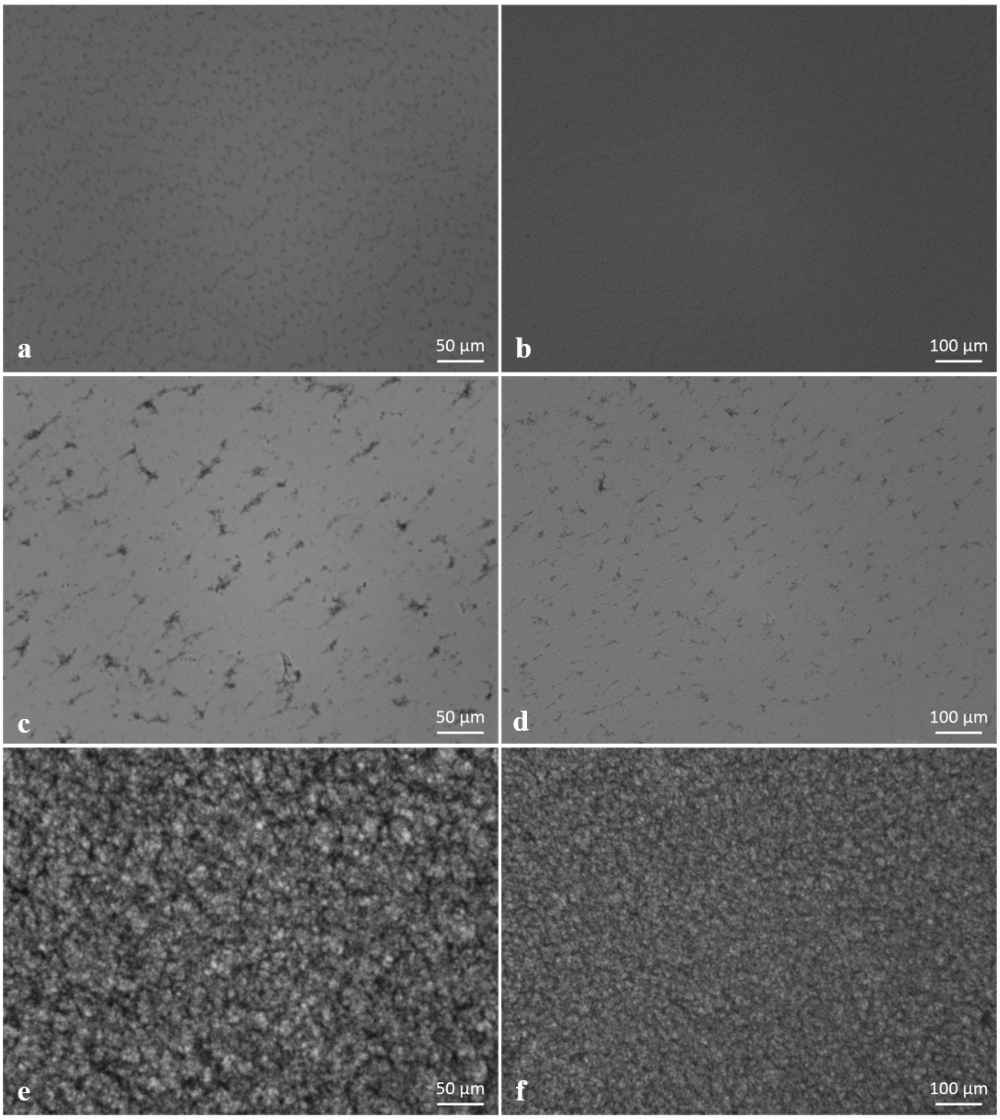

Figure 3.3.2.1. Optical images of RGO thin films deposited by spin-coating at (**a**,**b**) 1000 rpm, 60 s; (**c**,**d**) 200 rpm, 300 s; (**e**,**f**) rotational speeds increasing gradually from 200 rpm to 1300 rpm for 60 s each spinning step. Optical images have been taken at two different magnifications (**a**,**c**,**e**) 20×; (**b**,**d**,**f**) 10×.

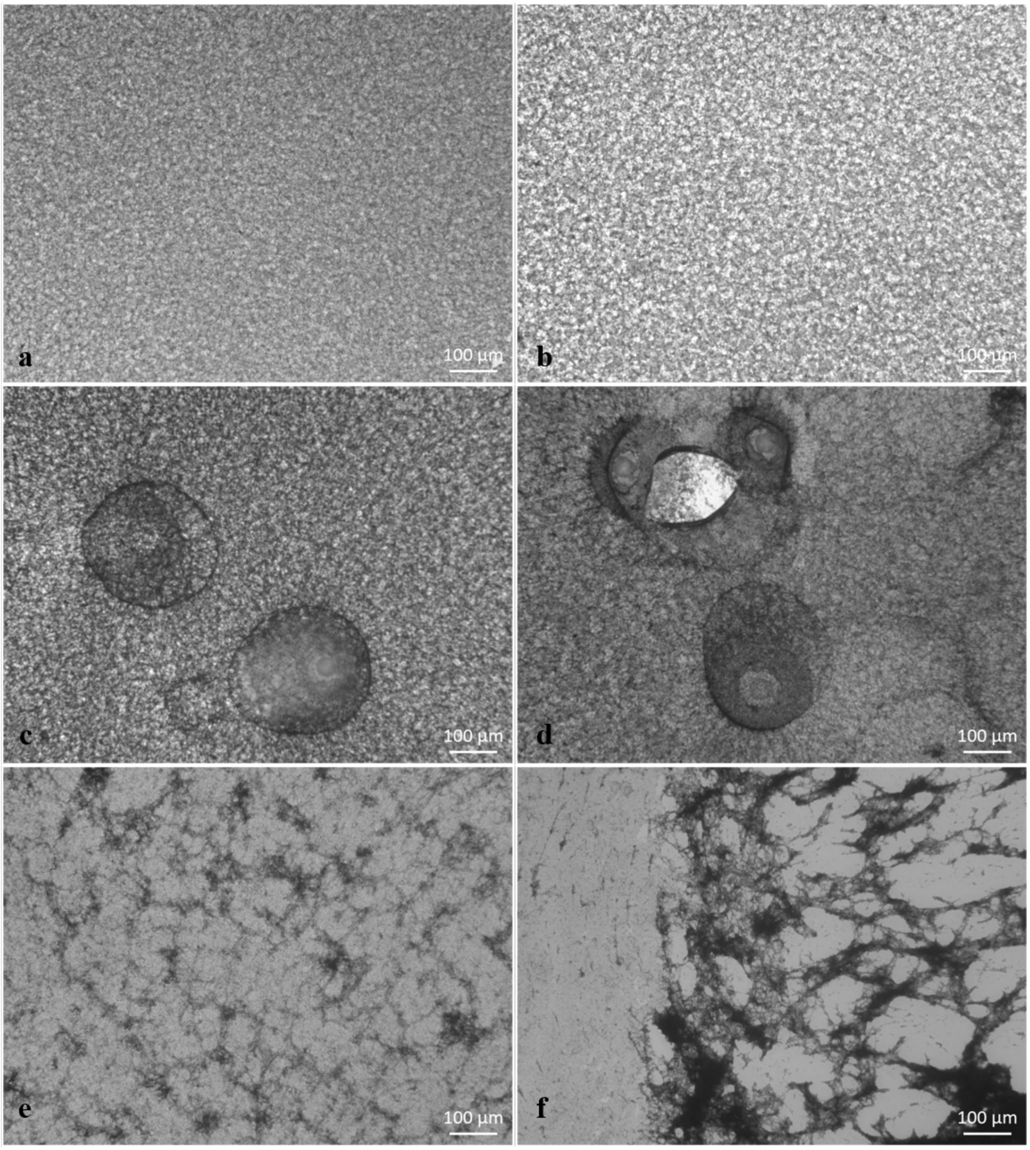

Figure 3.3.2.2. Optical images of RGO thin films deposited by drop-casting at (**a**) room temperature; (**b**) 50 °C; (**c**) 80 °C; (**d**) 100 °C; and (**e**) 200 °C. (**f**) Example of defects at the edge of films for a sample deposited at 110 °C. All images have a 10× magnification.

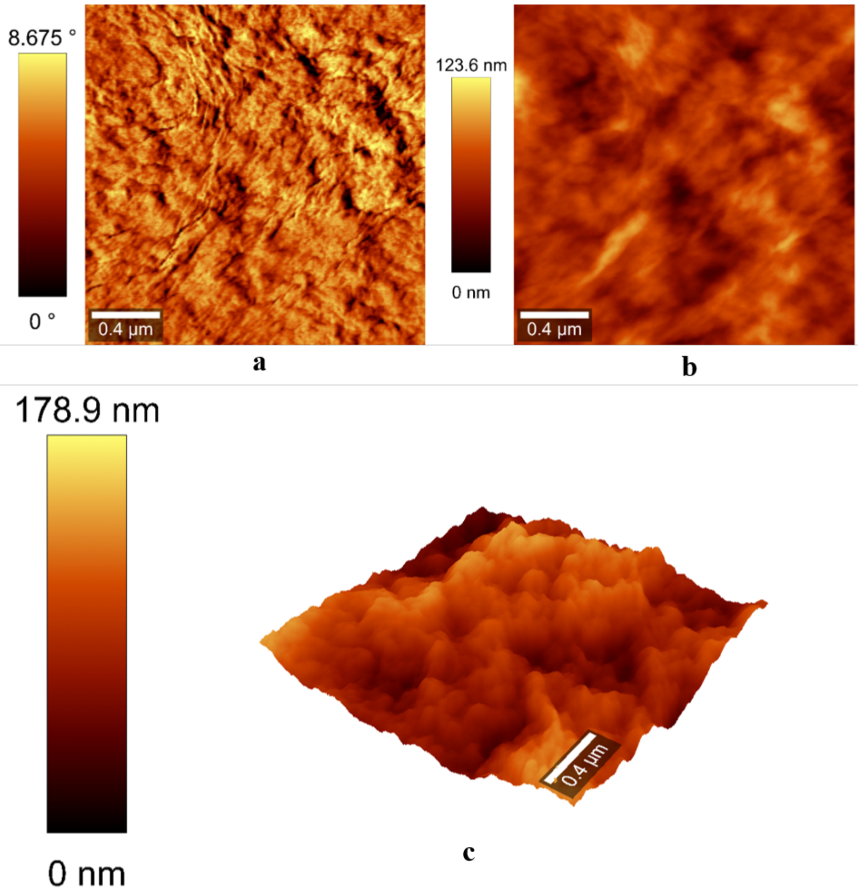

Figure 3.3.2.3. Atomic Force Microscopy images for RGO films deposited by drop-cast at room temperature. (**a**) phase; (**b**) topography; (**c**) topography 3D image.

3.4. Conclusions

We obtained stable RGO dispersions in water in concentrations higher than 0.05 mg/mL using a microwave-assisted hydrothermal synthesis method, by reducing GO in the presence of hydrazine hydrate and ammonia. The dispersions presented limited stability and were difficult to process as thin films, leading to random distribution of flakes on the substrate and random film morphologies. Unfortunately, RGO obtained using this protocol was not promising for our scope, which is blending with polymeric solution. Therefore, in the next chapter we employ an organic solvent, *N,N*-dimethylformamide, to develop a new synthesis method for RGO with potential applicability in developing polymer/RGO blended composites.

Chapter 4. Reduced Graphene Oxide in Dimethylformamide[2]

4.1. Background and Motivation

It has been already discussed in the literature that both pristine graphene and RGO could achieve colloidal stability in aqueous and organic solvents when using surfactants or stabilizing agents [7-9]. However, these are, in general, difficult to remove and might alter the properties and performance of the composites or the devices. There are, however, certain solvents with demonstrated ability to maintain stable dispersions of graphene in rather high concentrations without the aid of any dispersant agents [10]. We are speaking about solvents with surface energies similar to that of graphite basal plane, of ~70–80 mJ/m^2, and surface tensions of ~40–50 mJ/m^2. Thus, the best solvents to obtain stable RGO dispersions are *N*-methyl-pyrrolidone (NMP), *N,N*-dimethylformamide (DMF) and dimethyl sulfoxide (DMSO) [11].

In this chapter we aim to obtain stable dispersions of RGO in DMF using a microwave-assisted solvothermal method to reduce GO in DMF without using any other reducing or stabilizing agents. We had as reference a previous study for reducing GO in DMF using prolonged reflux (up to 72 hours) in a mixture of H_2O:DMF (1:9), without employing any reducing agents [12].

This chapter is entirely adapted from our previous publication [13] - R. Tarcan, M. Handrea-Dragan, O. Todor-Boer, I. Petrovai, C. Farcau, M. Rusu, A. Vulpoi, M. Todea, S. Astilean, and I. Botiz, "A new, fast and facile synthesis method for reduced graphene oxide in N,N-dimethylformamide," *Synthetic Metals,* vol. 269, p. 116576, 2020.

4.2. Materials and Methods

4.2.1. Optimization of the Solvothermal Reduction of Graphene Oxide in Water:DMF (1:9 v/v) with the Use of Microwaves

The first step in developing the here-presented method was the optimization of the method previously reported by Kim et al. [12] and its adaptation to the microwave-assisted solvothermal method. The GO dispersion in water:DMF (1:9) was subjected to microwave treatment in an Anton Paar

---

[2] This chapter is entirely adapted from our previous publication [13] - R. Tarcan, M. Handrea-Dragan, O. Todor-Boer, I. Petrovai, C. Farcau, M. Rusu, A. Vulpoi, M. Todea, S. Astilean, and I. Botiz, "A new, fast and facile synthesis method for reduced graphene oxide in N,N-dimethylformamide," *Synthetic Metals,* vol. 269, p. 116576, 2020.

Microwave 300 reactor for 30 minutes at 60, 80, 100, 120, and 140 °C. The obtained results are discussed in Section 4.3.1.

4.2.3. Synthesis of Reduced Graphene Oxide in Pure DMF

Following the optimization of the solvothermal reduction of graphene oxide in water:DMF (1:9 v/v) with the use of microwaves, we have employed a similar protocol for reducing GO dispersions of 0.5, 1, and 2 mg/mL in pure DMF. Each GO solution was subjected to microwave reduction for 30 minutes at 100, 120, 140 and 160 °C.

4.3. Results and Discussion

4.3.1. Optimization of the Solvothermal Reduction of GO in Water:DMF (1:9 v/v) with the Use of Microwaves

The previous study of Kim et al. [12] reported how long refluxing times (12, 24, and 27 h) of GO in a water:DMF mixture can lead to the formation of RGO as a black precipitate. By involving the microwaves in the process and reducing the reaction times, it was possible not only to make the whole process more efficient and facile, but also to obtain RGO homogenously dispersed in solution.

It was shown that the reduction process occurs only after treating the GO dispersions in water:DMF at temperatures as high as 120 and 140 °C. The success of the reaction was confirmed using UV-vis analysis.

4.3.2. Synthesis of GO and RGO Dispersions in Pure DMF

The preliminary observations following the microwave-assisted reduction of GO dispersions in DMF in concentrations of 0.5, 1, and 2 mg/mL at various temperatures, are summarized in Table 4.3.2.1. To assess the quality of resulting RGO after microwave treatment, we selected the GO solution of 1 mg/mL treated at 120 °C for 30 minutes after removing the few visible flakes, and used UV-vis and Raman spectroscopies to record the spectra in solution and thin films, respectively (Figure 4.3.2.3).

Table 4.3.2.1. Observations on the RGO dispersions in DMF after microwave assisted solvothermal reduction of GO in DMF. (Reproduced with permission from [13])

C_{GO} (mg/mL)	MW 100°C	MW 120°C	MW 140°C	MW 160°C
0.5	no flakes dark brown color	no flakes	many flakes	no dispersion
1	no flakes	very few flakes, removed after centrifugation or ultrasonication	no dispersion	no dispersion
2	no flakes	many flakes	no dispersion	not performed

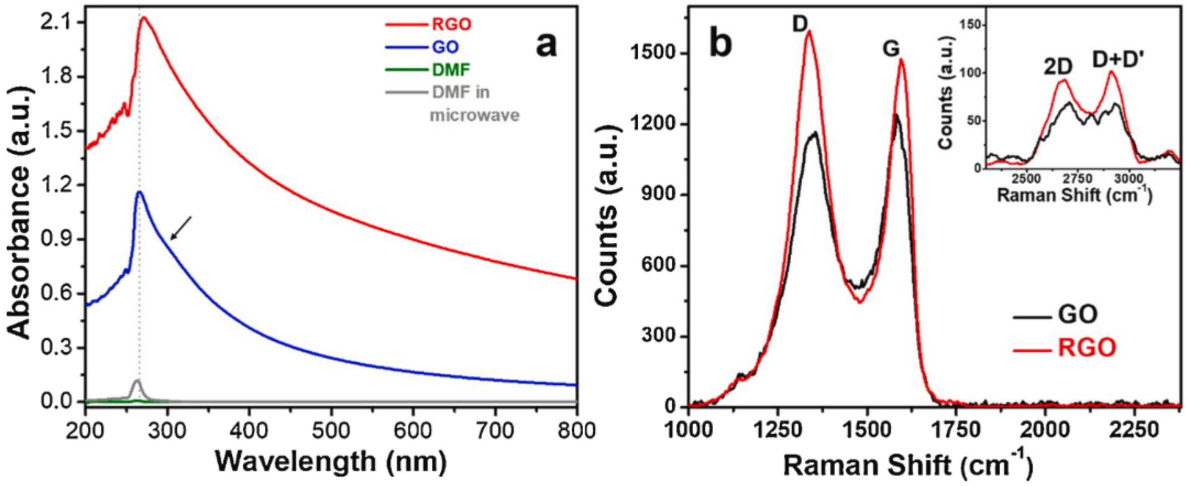

Figure 4.3.2.3. (**a**) UV-vis absorption spectra of GO, RGO and DMF before and after its microwave treatment. The vertical dotted grey line is for visual guidance. (**b**) Raman spectra of GO and RGO films deposited on a quartz substrate. The inset shows slightly smoothened Raman spectra corresponding to the 2300–3200 cm^{-1} spectral region. (Reproduced with permission from [13])

In the UV-vis spectra for GO, the absorption maximum, characteristic for π-π* transitions from C=C bonds, appears at ~265 nm, and the shoulder, characteristic for n-π* transitions resulting from C=O bonds, is visible at ~300 nm. On the other hand, in RGO, the maximum appears slightly red-shifted at ~271 nm, the shoulder disappears and the absorbance increases along the whole domain, indicating that the oxygen-containing groups were partially removed followed by a restoration of the sp^2 network. The UV-vis spectra for both samples looks unconventional compared to what we have seen for GO and RGO in water, and the reasons for these changes are explained in this thesis.

Raman spectra present the same two bands, D and G, and the ratio of these bands has been observed to increase from 0.93 in GO to 1.08 in RGO, indicating an increase in defective domains within the graphitic network, due to the elimination of oxygen-containing groups from the surface of the GO sheets, resulting in new vacancies and dislocations. Additionally, the 2D bands are showing at 2705 cm^{-1} in GO and 2675 cm^{-1} in RGO, indicating the graphene layer count, and D + D' bands are showing at 2930 cm^{-1} in GO and 2914 cm^{-1} in RGO, these bands being visible only in defective structures. The I_{2D}/I_G ratio can potentially reveal details about RGO layer count, and in our scenario, this ratio remains below 1, indicating a multi-layered RGO structure.

Scanning Electron Microscopy (SEM) images performed on drop-casted thin films for both GO and RGO indicated the presence of randomly aggregated and wrinkled flakes, with dimensions of ~8-10 μm. Transmission Electro Microscopy (TEM) images show individual wrinkled flakes of GO and RGO, and using Transmission Electron Microscopy Energy-Dispersive X-ray Spectroscopy (TEM-EDX) we have identified the chemical composition of these flakes and recorded an increase in the C/O ratio from 5.3 in GO to 7.9 in RGO, confirming once again the success of the reduction reaction.

X-ray Photoelectron Spectroscopy investigation shows significant changes in the spectrum after reduction. The intensities of the peaks resulting from C-C (sp^3) groups and from the oxygen containing groups are higher in GO and they are significantly decreased in RGO. Additionally, in the spectrum for RGO the peak resulting from C=C (sp^2) groups shows a significant increase compared to GO. These results indicate that the after the reduction process, sp^2 network is restored and the oxygen-containing groups have been partially removed, conclusion supported by the increase in C/O ratio from 0.61 in GO to 2.52 in RGO.

AFM images confirmed the multilayered structure of RGO, with the flakes stacked atop each other. Analysis of height cross-sectional profiles (Figure 4.3.2.6b) indicated that, on average, each RGO flake had a height of approximately 3.9 ± 0.5 nm, suggesting the possibility that each RGO flake consists of roughly 11 RGO sheets.

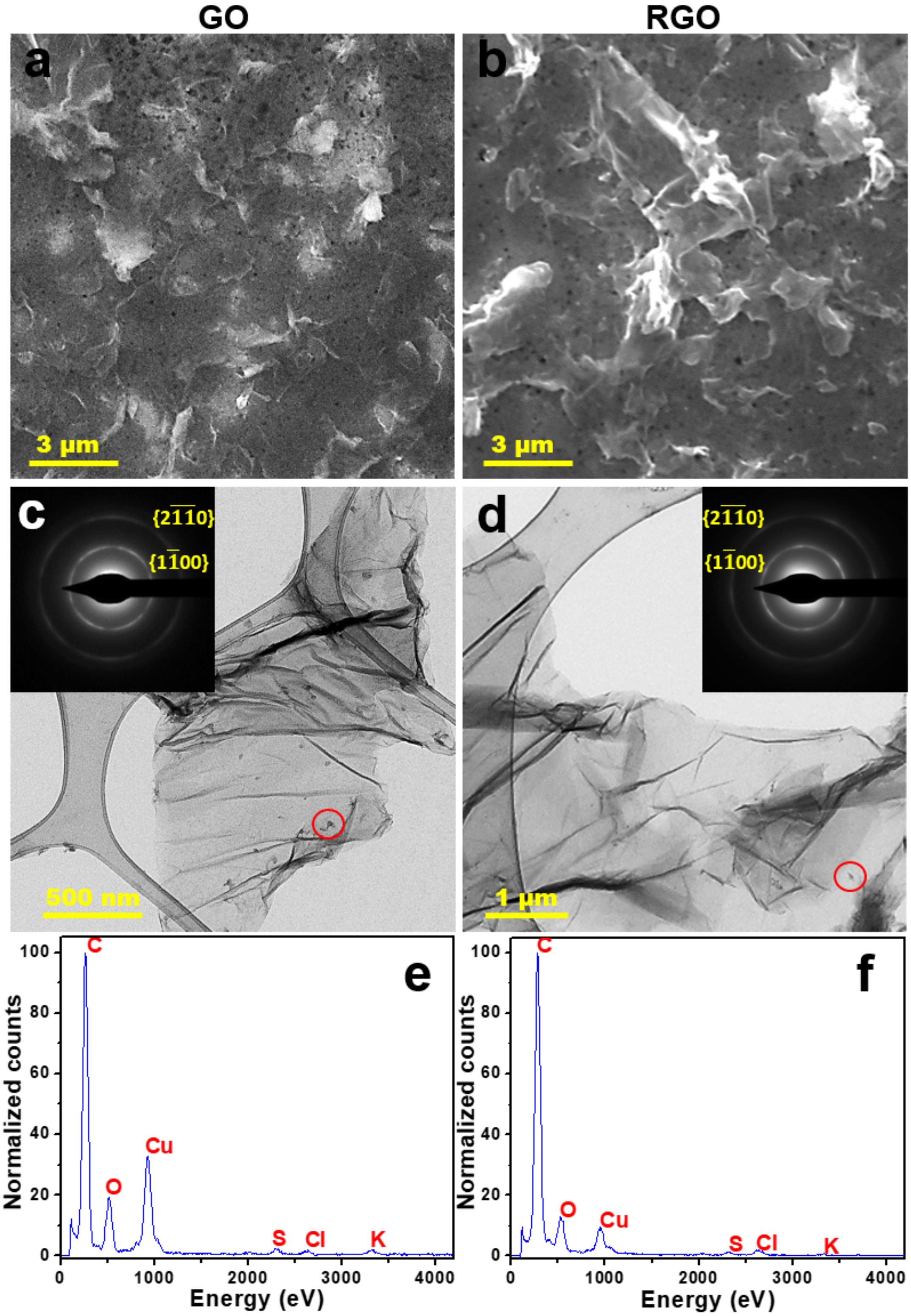

Figure 4.3.2.4. (**a**,**b**) SEM images of GO (**a**) and RGO (**b**). (**c**,**d**) TEM images of GO (**c**) and RGO (**d**). (**e**,**f**) TEM-EDX spectra for GO (**e**) and RGO (**f**). Insets in (**c**) and (**d**) are SAED images corresponding to GO and RGO, respectively. (Reproduced with permission from [13])

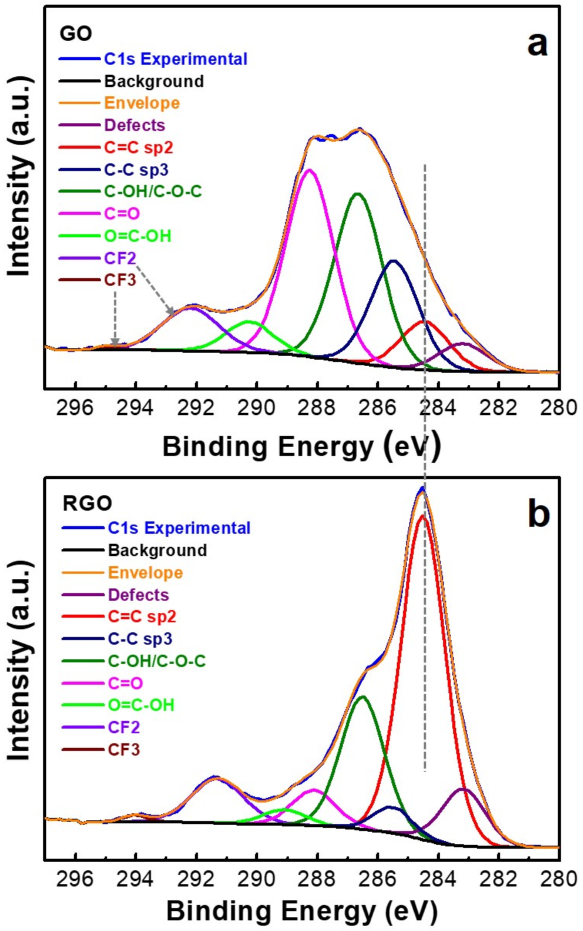

Figure 4.3.2.5. C1s XPS spectra of (**a**) GO and (**b**) RGO along with their corresponding deconvolutions. Dashed grey arrows indicate CF_2 and CF_3 moieties. The vertical dashed grey line is used for visual guidance. (Reproduced with permission from [13]).

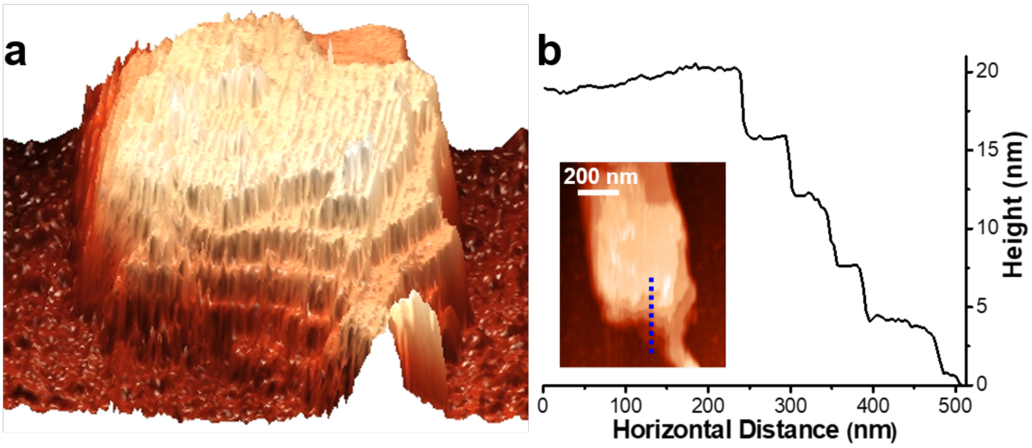

Figure 4.3.2.6. (**a**) 3D AFM height image depicting multilayered structure of RGO deposited on cover glass. (**b**) Height cross-sectional profile taken across the distance indicated by the blue dotted line in the inset (the AFM height image represents the image shown in (**a**)). Size of the image presented in (**a**) is roughly that of the inset displayed in (**b**). (Reproduced with permission from [13])

4.4. Conclusions

We report a new microwave-assisted solvothermal method to obtain stable dispersions of RGO in DMF in high concentration, by reducing a GO solution of 1 mg/mL, at 120 °C, for 30 min. Our method is more advantageous compared to others reported in the literature because (1) it implies only one solvent: DMF, (2) it does not involve additional reducing or stabilizing agents, (3) it leads to stable dispersions that can be processed as thin films, and (4) it is fast, easy, and cost-effective. Nonetheless, the method is promising for enhancing the dispersibility of RGO in other organic solvents and for developing new composite materials comprising RGO and polymers or other materials.

Chapter 5. Development of PMMA/RGO Composite Films as Thermal Interface Materials[3]

5.1. Background and Motivation

One of the biggest challenges arising from the miniaturization and integration of all kind of electronics into small, yet more powerful devices, is the development of new methods to efficiently dissipate the excessive heat produced by these devices. Thermal interface materials (TIM) are excellent candidates, thanks to their good thermal management properties. Moreover, RGO is also well-known for its unique properties similar to those of graphene, including good thermal conductivity. Thus, the objective of this chapter is to develop a new composite based on PMMA (polymethyl methacrylate) and RGO and to further explore its suitability for thermal management applications. The RGO dispersions obtained using the method reported in Chapter 4 are promising for developing such composites. Therefore, we used RGO stably dispersed in DMF as a carbon-filler and poly(methyl methacrylate) (PMMA) as a polymeric matrix. Only a small amount of RGO was incorporated in the RGO/PMMA composite, ensuring that the overall electrical resistivity of the composite remains near the values of neat PMMA.

This chapter is entirely adapted from our previous publication [14] - R. Tarcan, M. Handrea-Dragan, C.-I. Leordean, R. C. Cioban, G.-Z. Kiss, D. Zaharie-Butucel, C. Farcau, A. Vulpoi, S. Simon, and I. Botiz, "Development of polymethylmethacrylate/reduced graphene oxide composite films as thermal interface materials," *Journal of Applied Polymer Science,* vol. 139, p. e53238, 2022.

5.2. Materials and Methods

5.2.1. Sample Preparation

Composites of PMMA/RGO were generated by a simple method based on solution blending. Highly-concentrated solutions of PMMA in organic DMF were mixed with the RGO dispersion prepared also in DMF, resulting in polymeric composite mixtures with a content of RGO of 0.25 wt% and 0.5 wt%, respectively (PMMA+0.25%RGO and PMMA+0.5%RGO). For further characterization, we prepared thin films from drop-casting these solutions on glass substrates.

---

[3] This chapter is entirely adapted from our previous publication [14] R. Tarcan, M. Handrea-Dragan, C.-I. Leordean, R. C. Cioban, G.-Z. Kiss, D. Zaharie-Butucel, C. Farcau, A. Vulpoi, S. Simon, and I. Botiz, "Development of polymethylmethacrylate/reduced graphene oxide composite films as thermal interface materials," *Journal of Applied Polymer Science,* vol. 139, p. e53238, 2022, doi: https://doi.org/10.1002/app.53238

5.3. Results and Discussion

5.3.1. Experimental Results

Raman spectra for both PMMA and PMMA/RGO composites are shown in Figure 5.3.1.2. The spectra for PMMA shows multiple bands resulting from different vibration modes of the functional groups present in the molecule of PMMA. Significant differences are visible after the addition of RGO in the polymer matrix, when D and G bands appear at 1338 and 1598 cm^{-1}, respectively, indicating that the obtained PMMA/RGO film composites, contain RGO material that is homogeneously distributed in the final blending

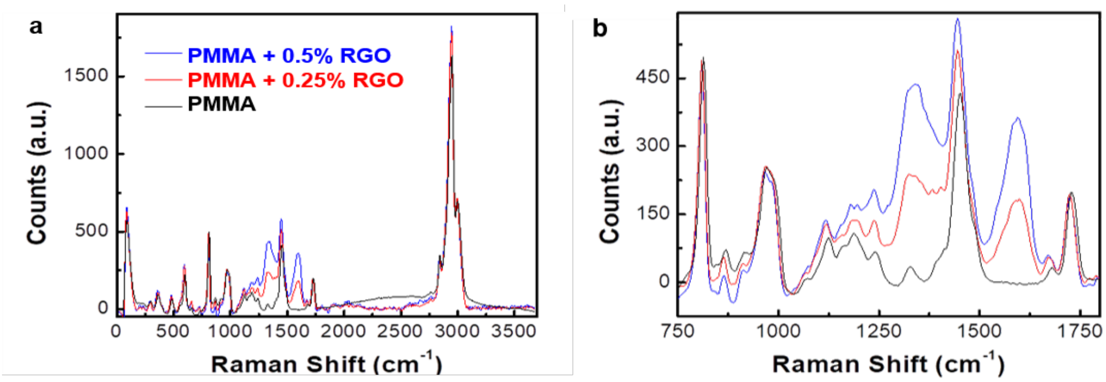

Figure 5.3.1.2. Typical Raman spectra acquired for PMMA, PMMA+0.25%RGO, and PMMA+0.25%RGO (**a**), and further normalized to the 812 cm^{-1} band (**b**). (Reproduced with permission from [14])

Further characterization involved SEM and AFM analysis of the thin films. SEM images presented in Figure 5.3.1.3a,b display homogenous films of both PMMA and PMMA/RGO composite. It can be observed that the PMMA film is smooth and relatively plain, without any significant features, while on the other hand, the PMMA/RGO composite film exhibits a rougher surface due to the presence of RGO sheets in the blend.

AFM images (Figure 5.3.1.3c–h) provide insights into the films microstructures, revealing important differences that exist between the surfaces of PMMA and that of PMMA/RGO films. Due to the presence of RGO sheets in the matrix, the film surface presents less pores, but relatively of larger size compared to the neat PMMA films where the pores were generally smaller and more densely packed. Additionally, the neat PMMA film presents a more amorphous structure, while the PMMA/RGO composite film displays bigger and more rigid features, due to the presence of rigid RGO flakes in the mixture and possibly due to the certain molecular aggregation that could occur around the carbonic structures.

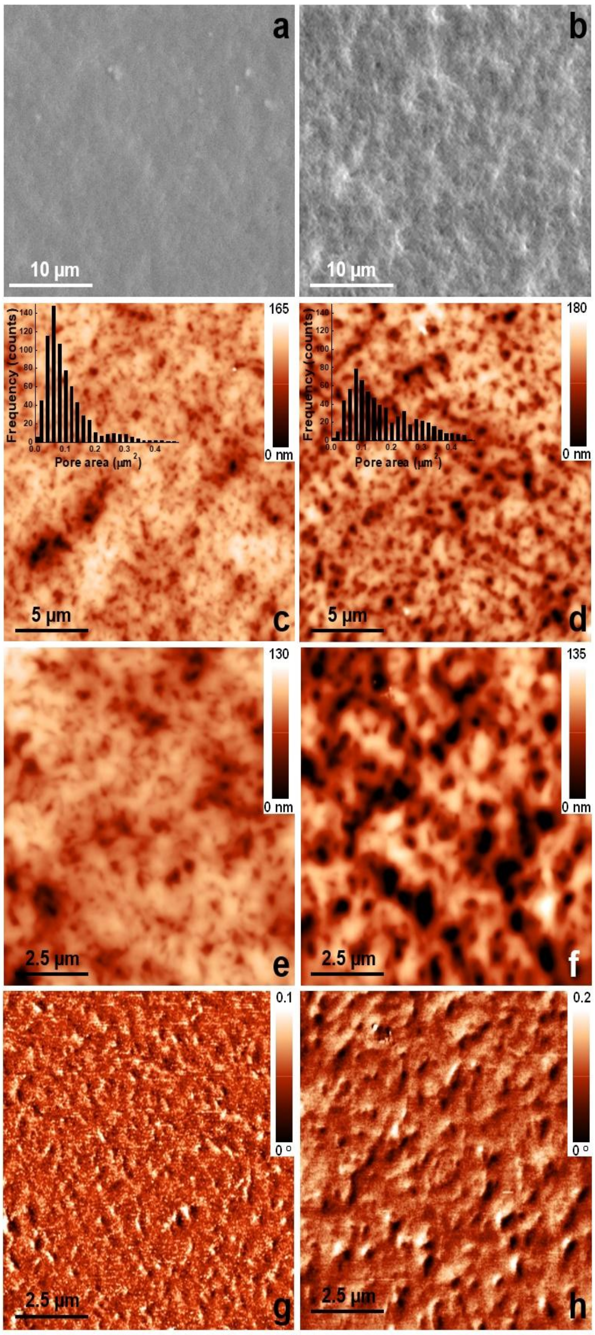

Figure 5.3.1.3. (**a**,**b**) SEM micrographs depicting PMMA (**a**) and PMMA+0.5%RGO (**b**) films deposited on solid glass substrate. (**c**–**h**) AFM topography (**c**–**f**) and phase (**g**–**h**) images emphasizing the surfaces of PMMA (**c**,**e**,**g**) and PMMA+0.5%RGO (**d**,**f**,**h**) films at different magnifications. Insets in (**c**) and (**d**) display pore size histograms that show random pores with different sizes on the two corresponding surfaces. (Reproduced with permission from [14])

Further, it was necessary to determine the thermoconductive properties of the PMMA/RGO composites and to evaluate their potential in developing thermal interface materials. Experimental measurements utilizing the transient hot bridge method were performed in order to determine both the thermal conductivity (k) and the specific heat capacity (c_p). The obtained results are summarized in Table 5.3.1.1 and correspond to the neat PMMA and PMMA/RGO composite films.

Table 5.3.1.1. Average experimental data values obtained for both PMMA and PMMA/RGO composite films and further used as an initial input for the numerical simulations. (Reproduced with permission from [14]).

Material	**k (W/mK)**	**c_p (J/kgK)**
PMMA	0.197425	1360.5
PMMA + 0.25% RGO	0.219725	1368.25
PMMA + 0.5% RGO	0.612667	1637

We recorded an increase in heat capacity and thermal conductivity of 0.6% and 11.3% respectively for PMMA+0.25%RGO, while for PMMA+0.5%RGO the increase in heat capacity was 20.3% and the thermal conductivity was increased by 210%, demonstrating that even a small amount of RGO can significantly improve the thermal properties of the composite.

5.3.2. Simulation Results

To evaluate both the efficiency and reliability of the newly fabricated TIMs based on PMMA/RGO composites, transient thermal simulations were conducted using TIMs not only in basic configuration but also in a realistic electronic assembly. Ansys Mechanical solver software was used to run the finite element simulation, while the resulting temperatures were used to evaluate the thermal performance of all studied TIMs.

Initially we considered a basic configuration “chip-TIM-heat sink” was comprised of a thermally-active silicon (Si) chip on top, an aluminum (Al) heat sink in the bottom, and a TIM with different thicknesses h of 0.1, 0.5 and 1 mm inserted between the first two. After the assessment of the impedance curves (Figure 5.3.2.1.), the results have shown that while increasing the RGO content in the sample, the steady state was achieved faster and thermal resistance R_{th} was lowered considerably for all TIMs, with a more pronounced decrease in R_{th} with increasing the TIM thickness.

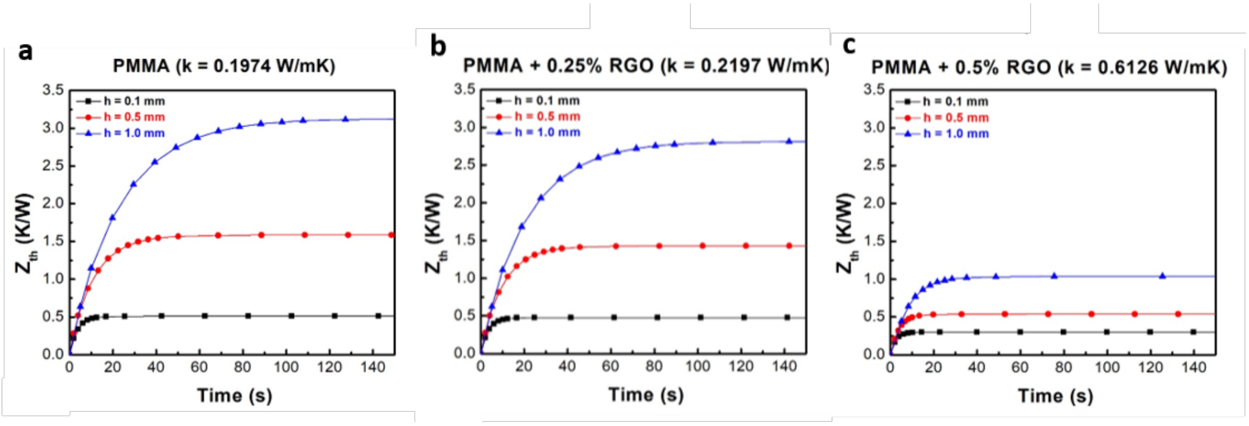

Figure 5.3.2.1. (a–c) Calculated thermal impedance curves (Z_{th}) determined for (**a**) neat PMMA, (**b**) PMMA+0.25%RGO and (**c**) PMMA+0.5%RGO TIM samples by taking into account various TIM thicknesses. (Reproduced with permission from [14])

To further evaluate the heat transfer performance of the novel TIMs developed from PMMA/RGO composite, in the second step we have focused our attention on a real life scenario, the so-called "assembly model LFPak56-PCB-TIM-heat sink". This model comprises a thermally active electric component, LFPak56, soldered on a six conductive-(Cu)layer printed circuit board (PCB), which was further attached to a heat sink ($AlSi_{12}Cu_1(Fe)$) via newly obtained TIMs of different thicknesses ($h = \{0.1, 0.5, 1 \text{ mm}\}$). In this study we have considered separately the two main cooling scenarios of the active systems: the bottom-side cooling through the PCB, and the top-side cooling through the mold.

In the bottom cooling scenario, all thermal impedance curves generated for each TIM case (Figure 5.3.2.3a–c) have shown that increasing the TIM thickness led to an increase of values of the final thermal impedance Z_{th}. This observation was explained by the longer heat path and the increased resistances that the generated heat meets while leaving the system. Moreover, it was also noticed that the steady state was obtained slower as the thickness of TIMs was increased. However, adding RGO into the system improves the overall thermal management with increasing the TIM thickness, and, considering the thermal time constants (Table 5.3.2.1), it leads to a shorter time to steady state of the entire assembly.

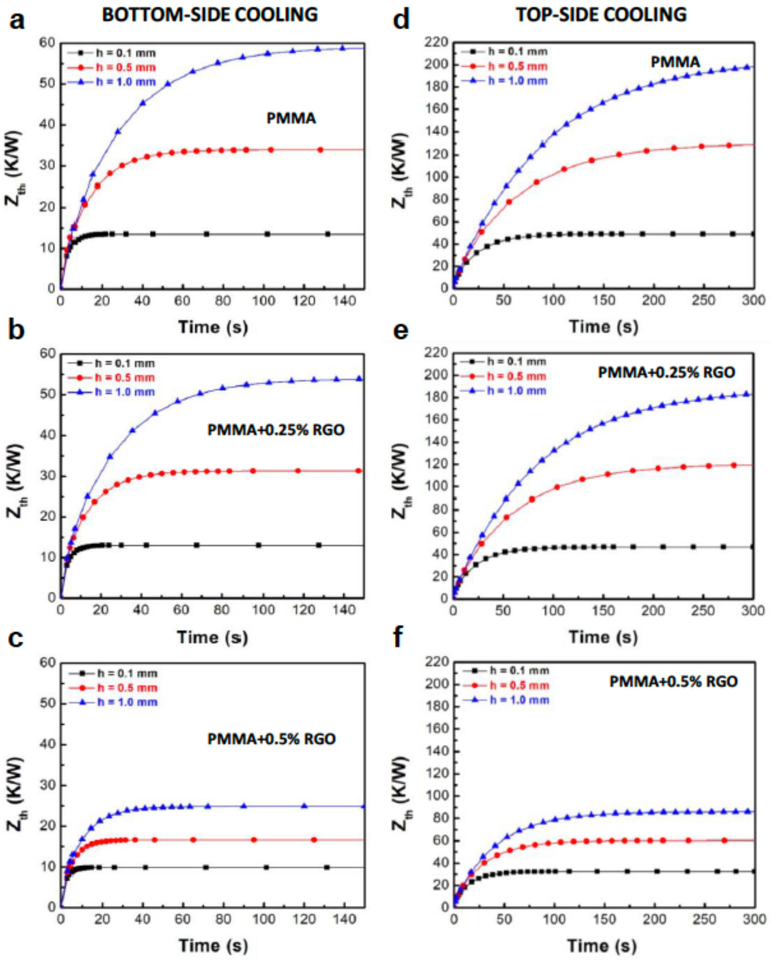

Figure 5.3.2.3. (**a**–**f**) Calculated thermal impedances Z_{th} corresponding to the bottom-side (**a**–**c**) and top-side (**d**–**f**) cooling LFPak56 configurations, acquired for different TIM samples exhibiting different thicknesses. (Reproduced with permission from [14])

Table 5.3.2.1. Thermal time constants as determined for the bottom-side cooling scenario. (Reproduced with permission from [14]).

	Thermal time constant (s)		
↓ **Material/Thickness** →	0.1 mm	0.5 mm	1 mm
PMMA	4.4	14.5	28.8
PMMA + 0.25% RGO	4.2	13.1	26.1
PMMA + 0.5% RGO	3.15	5.92	10.36

The calculated Z_{th} curves for the top-side case are depicted in Figure 5.3.2.3d–f and show very similar behavior as in the previous bottom-side scenario. However, the final R_{th} values did experience an about 4-fold increase, demonstrating a worse heat-management on this second separate route. Moreover, while the behavior of the thermal time constants was found to be rather similar with the values obtained for the bottom-side cooling scenario (Table 5.3.2.2), the overall values were about 3 times higher and thus suggested that the thermal steady state was achieved in a much slower manner as compared to the bottom-side cooling scenario.

Table 5.3.2.2. Thermal time constants as determined for the top-side cooling scenario. (Reproduced with permission from [14]).

	Thermal time constant (s)		
↓ **Material/Thickness** →	0.1 mm	0.5 mm	1 mm
PMMA	23.8	65.25	92.6
PMMA + 0.25% RGO	22.56	59.83	85.1
PMMA + 0.5% RGO	16.1	29.2	41.2

When compared to the bottom-side cooling case, the thermal performance in top-side case was significantly reduced. This can be explained through the fact that while in the former slug down case, the heat would travel from the silicon chip through the large copper slug on the bottom to a solder footprint and then to the cooled PCB, in this latter case, the heat has to pass to the TIM layer and heat sink through a rather poorly conductive mold material. Thus, despite the longer path, the increased conductivity of both the slug and footprint has made the bottom-side cooling scenario a much more efficient path for the heat. In addition to the better conduction, the slug down cooling through the PCB also took the advantage of a large heat capacity given by the copper layers that helped lower the chip temperature, and a large contact area to the heat sink.

5.4. Conclusions

We employed the RGO dispersion in DMF obtained using the microwave-assisted solvothermal method reported in the previous chapter to develop PMMA/RGO composites using a simple solution blending method. Raman, SEM, and AFM investigations confirmed that RGO is homogenously blended within the polymer matrix. We determined the thermoconductive properties of the composite and reported a 210% increase in thermal conductivity for the PMMA/RGO composite with only 0.5% RGO. We simulated the behavior of a PMMA/RGO-based TIM within an electronic assembly and showed that the thermal management is improved with the increased content of RGO and TIM thickness, especially in a bottom-side cooling model.

References:

[1] D. Li, M. B. Müller, S. Gilje, R. B. Kaner, and G. G. Wallace, "Processable aqueous dispersions of graphene nanosheets," *Nature Nanotechnology,* vol. 3, pp. 101-105, 2008, doi: 10.1038/nnano.2007.451

[2] T. Szabó, O. Berkesi, P. Forgó, K. Josepovits, Y. Sanakis, D. Petridis, and I. Dékány, "Evolution of Surface Functional Groups in a Series of Progressively Oxidized Graphite Oxides," *Chemistry of Materials,* vol. 18, pp. 2740-2749, 2006, doi: 10.1021/cm060258+

[3] A. Lerf, H. He, M. Forster, and J. Klinowski, "Structure of Graphite Oxide Revisited," *The Journal of Physical Chemistry B,* vol. 102, pp. 4477-4482, 1998, doi: 10.1021/jp9731821

[4] S. Stankovich, D. A. Dikin, R. D. Piner, K. A. Kohlhaas, A. Kleinhammes, Y. Jia, Y. Wu, S. T. Nguyen, and R. S. Ruoff, "Synthesis of graphene-based nanosheets via chemical reduction of exfoliated graphite oxide," *Carbon,* vol. 45, pp. 1558-1565, 2007, doi: https://doi.org/10.1016/j.carbon.2007.02.034

[5] M. Iliut, A.-M. Gabudean, C. Leordean, T. Simon, C.-M. Teodorescu, and S. Astilean, "Riboflavin enhanced fluorescence of highly reduced graphene oxide," *Chemical Physics Letters,* vol. 586, pp. 127-131, 2013, doi: https://doi.org/10.1016/j.cplett.2013.09.032

[6] S. Saxena, T. A. Tyson, S. Shukla, E. Negusse, H. Chen, and J. Bai, "Investigation of structural and electronic properties of graphene oxide," *Applied Physics Letters,* vol. 99, 2011, doi: 10.1063/1.3607305

[7] M. Lotya, Y. Hernandez, P. J. King, R. J. Smith, V. Nicolosi, L. S. Karlsson, F. M. Blighe, S. De, Z. Wang, I. T. McGovern, G. S. Duesberg, and J. N. Coleman, "Liquid Phase Production of Graphene by Exfoliation of Graphite in Surfactant/Water Solutions," *Journal of the American Chemical Society,* vol. 131, pp. 3611-3620, 2009, doi: 10.1021/ja807449u

[8] M. J. Fernández-Merino, J. I. Paredes, S. Villar-Rodil, L. Guardia, P. Solís-Fernández, D. Salinas-Torres, D. Cazorla-Amorós, E. Morallón, A. Martínez-Alonso, and J. M. D. Tascón, "Investigating the influence of surfactants on the stabilization of aqueous reduced graphene oxide dispersions and the characteristics of their composite films," *Carbon,* vol. 50, pp. 3184-3194, 2012, doi: https://doi.org/10.1016/j.carbon.2011.10.039

[9] P. Laaksonen, M. Kainlauri, T. Laaksonen, A. Shchepetov, H. Jiang, J. Ahopelto, and M. B. Linder, "Interfacial Engineering by Proteins: Exfoliation and Functionalization of Graphene by Hydrophobins," *Angewandte Chemie International Edition,* vol. 49, pp. 4946-4949, 2010, doi: https://doi.org/10.1002/anie.201001806

[10] Y. Hernandez, V. Nicolosi, M. Lotya, F. M. Blighe, Z. Sun, S. De, I. T. McGovern, B. Holland, M. Byrne, Y. K. Gun'Ko, J. J. Boland, P. Niraj, G. Duesberg, S. Krishnamurthy, R. Goodhue, J. Hutchison, V. Scardaci, A. C. Ferrari, and J. N. Coleman, "High-yield production of graphene by liquid-phase exfoliation of graphite," *Nature Nanotechnology,* vol. 3, pp. 563-568, 2008, doi: 10.1038/nnano.2008.215

[11] Y. Hernandez, M. Lotya, D. Rickard, S. D. Bergin, and J. N. Coleman, "Measurement of Multicomponent Solubility Parameters for Graphene Facilitates Solvent Discovery," *Langmuir,* vol. 26, pp. 3208-3213, 2010, doi: 10.1021/la903188a

[12] S. Kim, K. Choi, and S. Park, "Solvothermal reduction of graphene oxide in dimethylformamide," *Solid State Sciences,* vol. 61, pp. 40-43, 2016, doi: https://doi.org/10.1016/j.solidstatesciences.2016.07.013

[13] R. Tarcan, M. Handrea-Dragan, O. Todor-Boer, I. Petrovai, C. Farcau, M. Rusu, A. Vulpoi, M. Todea, S. Astilean, and I. Botiz, "A new, fast and facile synthesis method for reduced graphene oxide in N,N-dimethylformamide," *Synthetic Metals,* vol. 269, p. 116576, 2020, doi: https://doi.org/10.1016/j.synthmet.2020.116576

[14] R. Tarcan, M. Handrea-Dragan, C.-I. Leordean, R. C. Cioban, G.-Z. Kiss, D. Zaharie-Butucel, C. Farcau, A. Vulpoi, S. Simon, and I. Botiz, "Development of polymethylmethacrylate/reduced graphene oxide composite films as thermal interface materials," *Journal of Applied Polymer Science,* vol. 139, p. e53238, 2022, doi: https://doi.org/10.1002/app.53238

General Conclusions and Perspectives

In this thesis, we have first maximized the concentration in which we could obtain RGO stably dispersed in water. Even though the samples presented limited stability (< 24h) before the agglomeration of the flakes occurred, still this period of time is enough to make use of the obtained RGO in various technological applications.

We have further developed a new synthesis method for RGO in DMF using a simple microwave-assisted solvothermal method. Our method involves the reduction of GO in DMF dispersion in a microwave reactor at 120 °C in only 30 minutes without using any additional reducing or stabilizing agents.

We demonstrated the applicability of the RGO dispersion in DMF obtained using our method, and successfully developed new thermal interface materials based on PMMA/RGO composites.

We investigated the thermoconductive properties of the PMMA/RGO composite thin films and observed a 210% increase in thermal conductivity for the composite containing 0.5% RGO, demonstrating that even a small amount of RGO can significantly improve the thermal properties of the composite. Simulating the behavior of the composite as a TIM in an electronic assembly we demonstrated that the presence of RGO could have a major impact on the improvement in the thermal responses of the electronic system.

In the future, it is worth exploring the efficiency of the microwave-assisted solvothermal method for RGO synthesis in other organic solvents, such as N-methyl-pyrrolidone (NMP) or dimethylacetamide (DMAc). Nonetheless, the potential of the RGO dispersion in DMF in developing new TIMs can be further explored for its integration in other composites and devices.

Dissemination of the Research Results

List of ISI Publications Related to the Ph.D. Thesis

R. Tarcan, O. Todor-Boer, I. Petrovai, C. Leordean, S. Astilean, I. Botiz. “Reduced graphene oxide today.” *Journal of Materials Chemistry C*, vol. 8, pp. 1198-1224, 2020. **AIS: 1.163; IF: 6.4.**

R. Tarcan, M. Handrea-Dragan, O. Todor-Boer, I. Petrovai, C. Farcau, M. Rusu, A. Vulpoi, M. Todea, S. Astilean, I. Botiz. “A new, fast and facile synthesis method for reduced graphene oxide in *N,N*-dimethylformamide.” *Synthetic Metals,* vol. 269*,* p. 116576, 2020. **AIS: 0.479; IF: 4.4.**

R. Tarcan, M. Handrea-Dragan, C.-I. Leordean, R. C. Cioban, G.-Z. Kiss, D. Zaharie-Butucel, C. Farcau, A. Vulpoi, S. Simon, and I. Botiz, “Development of polymethylmethacrylate/reduced graphene oxide composite films as thermal interface materials” *Journal of Applied Polymer Science,* vol. 139, p. e53238, 2022. **AIS: 0.363; IF: 3.0.**

List of Other ISI Publications

O. Todor-Boer, I. Petrovai, **R. Tarcan**, L. David, S. Astilean, I. Botiz. “Control of microstructure in polymer: Fullerene active films by convective self-assembly.” *Thin Solid Films,* vol. 697, p. 137780, 2020. **AIS: 0.315; IF: 2.1.**

O. Todor-Boer, I. Petrovai**, R. Tarcan**, A. Vulpoi, L. David, S. Astilean, I. Botiz. “Enhancing photoluminescence quenching in donor-acceptor PCE11:PPCBMB films through the optimization of film microstructure.” *Nanomaterials,* vol. 9, p. 1757, 2019. **AIS: 0.7071; IF: 5.3.**

O. Todor-Boer, I. Petrovai, **R. Tarcan**, A-M. Craciun, L. David, S. B. Angyrus, S. Astilean, I. Botiz. “Altering the optoelectronic properties of neat and blended conjugated polymer films by controlling the process of film deposition.” *Journal of Optoelectronics & Advanced Materials,* vol. 21, p. 367, 2019. **AIS: 0.053; IF: 0.5.**

Participation in Scientific Conferences

R. Tarcan, O. Todor-Boer, I. Petrovai, L. David, S. Astilean, I. Botiz, "A study on reduced graphene oxide dispersion in water and influence of concentration on film quality", in *12th International Conference on Physics of Advanced Materials (ICPAM),* Heraklion, Greece, 22–28 September 2018 – poster presentation

R. Tarcan, M. Potara, O. Todor-Boer, I. Petrovai, S. Astilean, I. Botiz, "Dispersing reduced graphene oxide in organic solvent for optoelectronic devices", in *Interfaces in Organic and Hybrid Thin-Film Optoelectronics (INFORM Final Meeting),* Valencia, Spain, 5–7 March 2019 – poster presentation.

R. Tarcan, M. Handrea-Dragan, O. Todor-Boer, I. Petrovai, C. Farcau, M. Rusu, A. Vulpoi, M. Todea, S. Astilean, I. Botiz, "Synthesis of reduced graphene oxide in *N,N*-dimethylfomamide for future polymer-based composites", in *International Congress of Apollonia University XXXI Edition,* Iasi, Romania, 2 March 2021 – oral presentation (virtual session).

R. Tarcan, M. Handrea-Dragan, C.I. Leordean, R.C. Cioban, C. Farcau, A. Vulpoi, S. Simon, I. Botiz, "Improving thermal properties of PMMA/RGO composite thin films for thermal interfaces", in *International Congress of Apollonia University XXXII Edition,* Iasi, Romania, 28 February – 2 March 2022 – poster presentation.

Research Projects

Project Director

PN-III-P1-1.1-MC-2019-1557 – Research Mobility Project – at POLYMAT, Basque Center for Macromolecular Design & Engineering, University of Basque Country, Donostia–San Sebastian, Spain, 11 November – 9 December 2019.

Research Assistant

PN-III-P4-ID-PCE-2016-0837, at Interdisciplinary Research Institute in Bio-Nanophotonics, Babes-Bolyain University, Cluj-Napoca, Romania, December 2018 – December 2019.

PN-III-CERC-CO-PED-2-2019, at Interdisciplinary Research Institute in Bio-Nanophotonics, Babes-Bolyain University, Cluj-Napoca, Romania, September 2020 – September 2021.